

Capturing anharmonic effects in single vibronic level fluorescence spectra using local harmonic Hagedorn wavepacket dynamics

Zhan Tong Zhang, Máté Visegrádi, and Jiří J. L. Vaníček^{a)}

Laboratory of Theoretical Physical Chemistry, Institut des Sciences et Ingénierie Chimiques, Ecole Polytechnique Fédérale de Lausanne (EPFL), CH-1015 Lausanne, Switzerland

(Dated: 23 August 2024)

Hagedorn wavepacket dynamics yields exact single vibronic level (SVL) fluorescence spectra from any initial vibrational level in displaced, squeezed, and Duschinsky-rotated global harmonic models. Real molecules, however, have anharmonic potential energy surfaces. To partially describe effects of anharmonicity on the spectra, we combine the Hagedorn approach to spectroscopy with the local harmonic approximation of the potential. We compute the SVL spectra for several anharmonic Morse-type potentials in one, two, and twenty dimensions and compare them to the results of global harmonic approximations and, where possible, of exact quantum calculations. We show that the local harmonic approach yields more accurate results than global harmonic approximations, especially for the emission spectra from higher initial vibrational levels.

I. INTRODUCTION

Single vibronic level (SVL) fluorescence spectroscopy has been used to study intramolecular relaxation,^{1–4} characterize molecular vibronic structure,^{5,6} and identify conformers and reactive intermediates.^{7–9} Recently, several time-dependent approaches to simulate SVL spectra in global harmonic models have been developed.^{10–13} For example, Tapavicza¹¹ used a generating function formalism to compute the SVL spectra of anthracene from singly excited levels using a harmonic model determined from accurate electronic structure calculations. Motivated by Tapavicza’s work, we proposed a method based on Hagedorn wavepacket dynamics,^{14–16} which enabled us to compute the SVL spectra from any initial vibrational levels¹² and to simulate the SVL spectra of higher vibrational levels of anthracene within the harmonic approximation.¹³

To accurately compute vibrationally resolved spectra of polyatomic molecules, however, it is often necessary to account for the anharmonicity of the molecular potential energy surfaces (PESs).^{17–23} Conventional time-independent methods that evaluate Franck–Condon factors for each transition can include anharmonic effects by using the variational principle^{24–27} or perturbation theory.^{18,28,29} In higher-dimensional systems with Duschinsky coupling, the determination of anharmonic wavefunctions and the computation of a large number of Franck–Condon overlaps become very costly or even unfeasible. Even when feasible, computing all Franck–Condon factors is wasteful because individual peaks are not visible in low- or intermediate-resolution spectra.

Alternatively, in the time-dependent framework, the spectrum is computed as the Fourier transform of an appropriate autocorrelation function obtained by propagating a wavepacket on the final electronic PES.^{30,31} Semi-classical trajectory-based methods can capture the effects

of an anharmonic PES more efficiently using an on-the-fly implementation that relies only on the local PES information. In the thawed Gaussian approximation^{32–35} (TGA), a Gaussian wavepacket is propagated using the local harmonic approximation (LHA), which expands the true potential locally to the second order at each time step. The center of the wavepacket then follows the anharmonic classical trajectory, while the width evolves according to the local Hessian matrix.

Whereas the TGA uses a single Gaussian wavepacket to simulate the emission or absorption process from the ground vibrational level,^{34,36–38} our approach,^{12,13} based on Hagedorn wavepackets,^{14–16,39} uses functions that are polynomials multiplied by a Gaussian to compute SVL spectra from any vibrationally excited levels. These functions result from applying a special raising operator to a Gaussian wavepacket. Remarkably, the Hagedorn functions are not only exact solutions of the time-dependent Schrödinger equation (TDSE) in global harmonic models, but they remain so even with a state-dependent quadratic potential. This property enables an efficient combination of Hagedorn wavepacket dynamics with the local harmonic approximation in order to partially account for anharmonic effects in SVL spectra.

Here, we first apply the local harmonic Hagedorn wavepacket approach to simulate SVL spectra from different initial vibrational levels in a one-dimensional Morse potential and in a two-dimensional coupled Morse system. Compared to the quantum split-operator results, the local harmonic spectra improve on both vertical and adiabatic harmonic models; however, significant differences from the exact results still exist for spectra with high initial excitations. In a twenty-dimensional coupled Morse system, we demonstrate the practicality of the Hagedorn approach in higher dimensions and the importance of anharmonic effects by comparing the local and global harmonic results.

^{a)}Electronic mail: jiri.vanicek@epfl.ch

II. THEORY

In single vibronic level fluorescence spectroscopy, the molecular population in the ground electronic state g is first excited to a specific vibrational level $|K\rangle \equiv |e, K\rangle$ in an electronically excited state e , where $K = (K_1, \dots, K_D)$ is a multi-index of non-negative integers specifying the vibrational quantum numbers in the D vibrational degrees of freedom. The rate of subsequent spontaneous emission from this vibronic level with energy $\hbar\omega_{e,K}$ is given by the Fourier transform^{11,30,31}

$$\sigma_{\text{em}}(\omega) = \frac{4\omega^3}{3\pi\hbar c^3} |\mu_{ge}|^2 \text{Re} \int_0^\infty \overline{C(t)} \exp[it(\omega - \hbar\omega_{e,K})/\hbar] dt \quad (1)$$

of the wavepacket autocorrelation function

$$C(t) = \langle K | \exp(-iH_g t/\hbar) | K \rangle, \quad (2)$$

obtained by propagating the initial wavepacket with the ground-state Hamiltonian H_g . We make the Condon approximation, in which the transition dipole moment μ_{ge} does not depend on nuclear coordinates.

Assuming the harmonic approximation for the excited-state surface V_e , we can represent the initial vibrational wavepacket $|K\rangle$ by a Hagedorn function¹²

$$\varphi_K = (K!)^{-1/2} (A^\dagger)^K \varphi_0, \quad (3)$$

obtained by applying Hagedorn's raising operator¹⁴

$$A^\dagger := \frac{i}{\sqrt{2\hbar}} \left(P_t^\dagger \cdot (\hat{q} - q_t) - Q_t^\dagger \cdot (\hat{p} - p_t) \right) \quad (4)$$

to the D -dimensional normalized Gaussian, parametrized in the excited-state normal-mode coordinates as

$$\begin{aligned} \varphi_0(q) &= \frac{1}{(\pi\hbar)^{D/4} \sqrt{\det(Q_t)}} \\ &\times \exp \left\{ \frac{i}{\hbar} \left[\frac{1}{2} x^T \cdot P_t \cdot Q_t^{-1} \cdot x + p_t^T \cdot x + S_t \right] \right\}. \end{aligned} \quad (5)$$

Here, $x := q - q_t$ is the shifted position, q_t and p_t are the position and momentum of the center of the wavepacket in the phase space, and S_t is the classical action. Compared to Heller's parametrization,^{32,40} the width matrix $C_t \equiv P_t \cdot Q_t^{-1}$ of the Gaussian is factorized in terms of two complex-valued D -dimensional matrices Q_t and P_t , which satisfy the symplecticity conditions^{16,39}

$$Q_t^T \cdot P_t - P_t^T \cdot Q_t = 0 \quad \text{and} \quad (6)$$

$$Q_t^\dagger \cdot P_t - P_t^\dagger \cdot Q_t = 2i\text{Id}, \quad (7)$$

where Id is the D -dimensional identity matrix. In Eq. (3), we used the multi-index notation for $K! = K_1! \cdot K_2! \cdot \dots \cdot K_D!$ and $(A^\dagger)^K = (A_1^\dagger)^{K_1} \cdot (A_2^\dagger)^{K_2} \cdot \dots \cdot (A_D^\dagger)^{K_D}$, where A_j^\dagger is the j -th component of the vector operator A^\dagger .

In the position representation, Hagedorn functions (3) are given by polynomials multiplying a common Gaussian (5) and form an orthonormal basis. Instead of

using them as a time-dependent basis as in previous applications,⁴¹⁻⁴⁵ here we exploit the fact that they are exact solutions to the TDSE with a time-dependent harmonic potential that may depend on the state of the system.

To partially capture anharmonic effects while maintaining the simplicity of the propagation, we use the local harmonic approximation (LHA), where the true potential V is expanded as an effective quadratic potential,

$$V_{\text{LHA}}(q; q_t) := V(q_t) + V'(q_t) \cdot x + x^T \cdot V''(q_t) \cdot x/2, \quad (8)$$

around the center q_t of the wavepacket at each time.

Solving the TDSE with the Hagedorn functions and LHA yields the following equations of motion for the parameters of the guiding Gaussian φ_0 from Eq. (5):

$$\begin{aligned} \dot{q}_t &= m^{-1} \cdot p_t, & \dot{p}_t &= -V'(q_t) \\ \dot{Q}_t &= m^{-1} \cdot P_t, & \dot{P}_t &= -V''(q_t) \cdot Q_t, \\ \dot{S}_t &= L_t, \end{aligned} \quad (9)$$

with m being the real symmetric mass matrix and L_t the Lagrangian.^{16,39} The center of the wavepacket is guided by the classical trajectory and can explore the anharmonic shape of the PES. The local quadratic expansion takes into account the changes of the Hessian $V''(q_t)$ along the anharmonic trajectory while ensuring that the form (i.e., the multi-index K) of the Hagedorn function remains constant. Remarkably, the classical-like equations (9) are exactly the equations of motion in the thawed Gaussian approximation and do not depend on the initial excitation K . As such, the SVL spectra from any vibrational levels may be obtained from a single Gaussian trajectory, and in *ab initio* applications, the expensive on-the-fly electronic structure calculations do not have to be repeated for different K .

To evaluate the autocorrelation function (2), it is necessary to compute overlaps between arbitrary two Hagedorn functions. Unlike for overlaps between two Gaussians, we have not found a simple, closed-form expression for overlaps of Hagedorn functions. Instead, we evaluate these overlaps with the exact, recursive algebraic expressions derived in Ref. 46, and thus avoid errors and difficulties arising from the use of numerical quadratures.⁴⁷

III. NUMERICAL EXAMPLES

In the following, we use mass-scaled nuclear normal-mode coordinates and the atomic units ($\hbar = 1$).

A. One-dimensional Morse potential

Using the Morse oscillator as the first example of a realistic anharmonic potential, we assume that the final, ground electronic surface V_g is given by

$$V_g(q) = \frac{\omega_g}{4\chi} \left[1 - e^{-\sqrt{2m\omega_g\chi}(q - q_{\text{eq},g})} \right]^2, \quad (10)$$

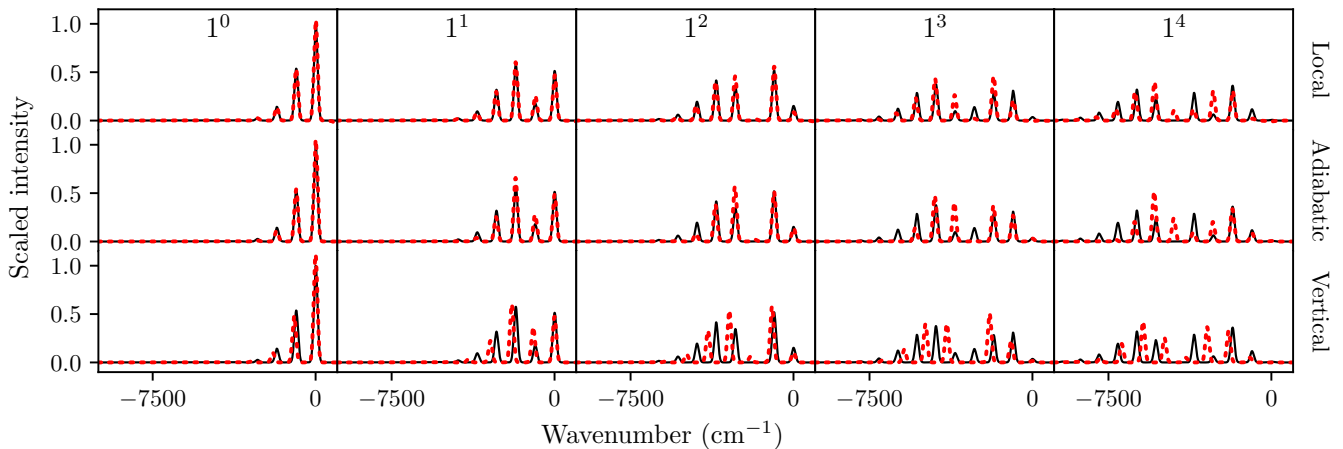


FIG. 1. SVL spectra computed with Hagedorn wavepackets (red dashed lines) propagated using the local, adiabatic, or vertical harmonic approximation of a one-dimensional Morse potential are compared to exact quantum spectra (black solid lines); the initial vibrational excitation is indicated at the top.

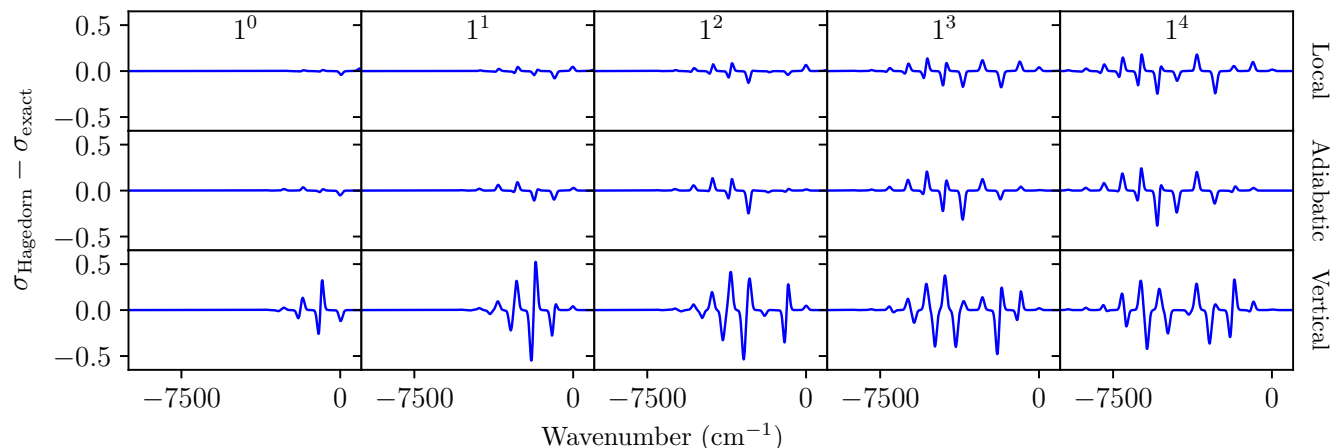


FIG. 2. Differences ($\sigma_{\text{Hagedorn}} - \sigma_{\text{exact}}$) between the SVL spectra of a one-dimensional Morse potential computed with Hagedorn wavepacket dynamics and the corresponding exact spectra. See the caption of Fig. 1 for more details.

where $q_{\text{eq},g} = 15$ is the equilibrium position, $\omega_g = 0.0041$ is the frequency of the harmonic oscillator fitted at $q_{\text{eq},g}$, and $\chi = 0.002$ is a dimensionless anharmonicity parameter. The initial wavepacket $|K\rangle$ is assumed to be an eigenfunction of a harmonic potential V_e that has a fundamental frequency of $\omega_e = 0.00456$ and is centered at the excited-state equilibrium position $q_{\text{ref},e} = 0$.

To quantify the anharmonic effects, two global harmonic models were constructed for V_g . In the vertical harmonic approximation (VHA), the effective potential was constructed around the Franck-Condon point as

$$V_{\text{VHA}} = V_g(q_{\text{eq},e}) + V_g'(q_{\text{eq},e}) \cdot (q - q_{\text{eq},e}) + (q - q_{\text{eq},e})^T \cdot V_g''(q_{\text{eq},e}) \cdot (q - q_{\text{eq},e})/2, \quad (11)$$

whereas in the adiabatic harmonic approximation (AHA), the potential was expanded around the ground-

state equilibrium position $q_{\text{eq},g}$ as

$$V_{\text{AHA}} = V_g(q_{\text{eq},g}) + (q - q_{\text{eq},g})^T \cdot V_g''(q_{\text{ref},g}) \cdot (q - q_{\text{eq},g})/2, \quad (12)$$

where the gradient $V_g'(q_{\text{eq},g})$ vanishes at the equilibrium configuration.

Figure 1 compares the SVL spectra (from 1^a levels, where a is the vibrational quantum number of the initial state) computed using the Hagedorn wavepacket approach combined with the local, adiabatic, and vertical harmonic approximations. These spectra are compared with exact quantum results to assess the accuracy of various approximations of the anharmonic Morse potential. The split-operator quantum calculations were performed on a position grid with 2048 equidistant points between -128 and 356 . The differences between exact and ‘‘Hagedorn’’ spectra are shown in Fig. 2.

In all simulations, the propagation lasted 80000 a.u.

(20000 steps with a time step of 4 a.u.) and the correlation function (2) was computed every five steps. Whereas the quantum calculation required a separate propagation of the wavepacket for each excitation level, in the Hagedorn approach it is sufficient to propagate only the ground-level Gaussian wavepacket to generate spectra for all excitation levels. The spectra were broadened by a Gaussian function with a half-width at half-maximum of 100 cm^{-1} . Intensities were scaled to the highest peak of the 1^0 quantum spectrum, and the wavenumbers were shifted so that the transition to the ground level (1_0^a) on the ground-state surface was at 0 cm^{-1} .

For the ground-level emission spectra from 1^0 (first column in Figs. 1 and 2), both the adiabatic and local harmonic models show excellent agreement with the quantum results. The vertical model also performs reasonably well; however, the spacing between the peaks differs slightly from the exact spectrum, which could be corrected with an empirical scaling factor. In the 1^1 and 1^2 spectra (second and third columns), the local and adiabatic harmonic models still perform well, with the LHA spectra capturing slightly better the small peaks at lower wavenumbers.

As the initial excitation increases, the vertical harmonic model breaks down further, and significant differences from the exact spectra become apparent both in the intensities and peak positions. The adiabatic and local harmonic models still provide reasonable results, but they too start to deviate from the quantum benchmarks. This is expected since the initial states with higher vibrational excitations are more delocalized and feel more the anharmonic shape of the potential. We also observe several small, unphysical negative peaks in the LHA spectra due to the nonconservation of energy and the nonlinearity of the TDSE in the local harmonic dynamics.^{36,37,40} Nonetheless, compared to the results of global harmonic models, the local harmonic results generally differ less from the exact spectra, especially in the lower frequency region (see Fig. 2). This region corresponds to transitions to higher vibrational levels, which are more significantly affected by the anharmonicity of the ground-state PES. In contrast, the adiabatic harmonic model tends to perform slightly better in the higher frequency range for transitions to vibrational levels closer to the harmonic region.

B. Two-dimensional coupled Morse potential

In one-dimensional systems, Hagedorn functions reduce to Hermite polynomials multiplied by a Gaussian;¹⁴ the beauty of the Hagedorn wavepackets emerges in higher dimensions, where they are not simple products of one-dimensional Hermite functions.^{16,48} Remarkably, they still preserve their form and remain exact solutions to the TDSE with a global or local harmonic potential, even in the presence of Duschinsky rotation (mode mixing).

To validate the local harmonic Hagedorn dynamics in a multidimensional anharmonic system, we used the “coupled Morse potential.”⁴⁹ This nonseparable generalization of the Morse potential to higher dimensions is given by

$$V_g(q) = \sum_{j=1}^D V_j(q_j) + V_{\text{cpl}}(q). \quad (13)$$

In each vibrational degree of freedom j , there is a Morse term V_j in the form of Eq. (10) specified by parameters $\omega_{g,j}$, χ_j , and $q_{\text{eq},g,j}$. A D -dimensional coupling term,

$$V_{\text{cpl}}(q) = d' \left(1 - e^{-a^T \cdot (q - q_{\text{eq},g})} \right)^2, \quad (14)$$

introduces nonseparability and depends on the dissociation energy d' and a vector $a \equiv (a_1, \dots, a_D)$ of decay parameters, which are related by a dimensionless anharmonicity vector $\chi' \equiv (\chi'_1, \dots, \chi'_D)$ via $a = \sqrt{8d'} \chi'$.

A two-dimensional Morse system with $\omega_g = (0.0041, 0.005)$, $\chi = (0.005, 0.002)$, $q_{\text{eq},g} = (20, 5)$, $d' = 0.08$ and $\chi' = (0.001, 0.001)$ was chosen as the simplest multidimensional example. The harmonic excited-state PES is centered at $q_{\text{eq},e} = (0, 0)$ and its Hessian corresponds to fundamental frequencies $\omega_e = (0.00456, 0.00365)$.

We used the local harmonic Hagedorn dynamics to compute the emission spectra from levels 1^{02^0} , 1^{02^2} , 1^{12^1} , and 1^{32^1} . Exact quantum split-operator calculations (with 256×256 position grid points ranging from -128 to 356 in each dimension) as well as simulations using the adiabatic and vertical harmonic approximations [Eqs. (12) and (11)] were performed for comparison. The time step, total propagation time, and frequency of evaluating the autocorrelation function were the same as in the one-dimensional Morse model.

The simulated spectra were broadened with a Gaussian function with a half-width at half-maximum of 100 cm^{-1} . The intensities in the spectra were scaled by the intensity of the highest peak in the exact 1^{02^0} spectrum, and the wavenumbers were shifted so that the transition to the ground level in the ground state was at 0 cm^{-1} .

Figure 3 compares the spectra computed using the different approximations with the exact quantum spectra and the differences are shown in Fig. 4. In this two-dimensional system, the spectra already become quite complex, but the behavior of the different approximations mirrors that of the one-dimensional case. Both local and adiabatic harmonic results agree very closely with the exact ground-level emission spectrum (1^{02^0}), whereas the vertical harmonic spectrum reproduces the intensities relatively well but has wrong peak spacing.

The effect of anharmonicity becomes more pronounced for higher initial vibrational excitations, leading to increased deviations of both local and global harmonic results from the exact spectra. At the same level of initial excitation in a single mode, the global harmonic models perform better when mode 2 is excited than when mode

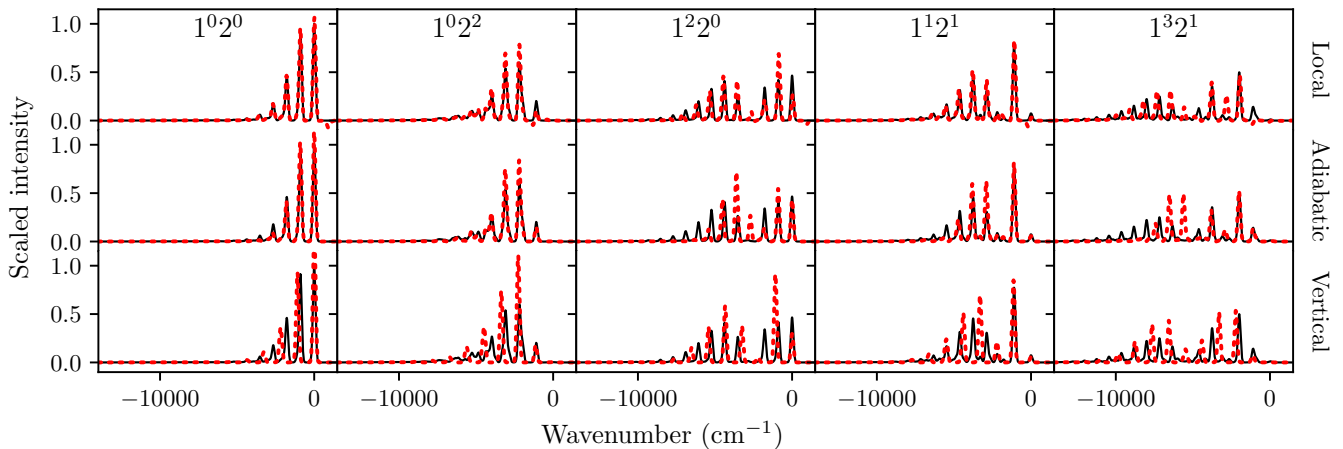


FIG. 3. SVL spectra computed with Hagedorn wavepackets (red dashed lines) propagated using the local, adiabatic, or vertical harmonic approximation of a two-dimensional coupled Morse potential are compared to exact quantum spectra (black solid lines); the initial vibrational excitation is indicated at the top.

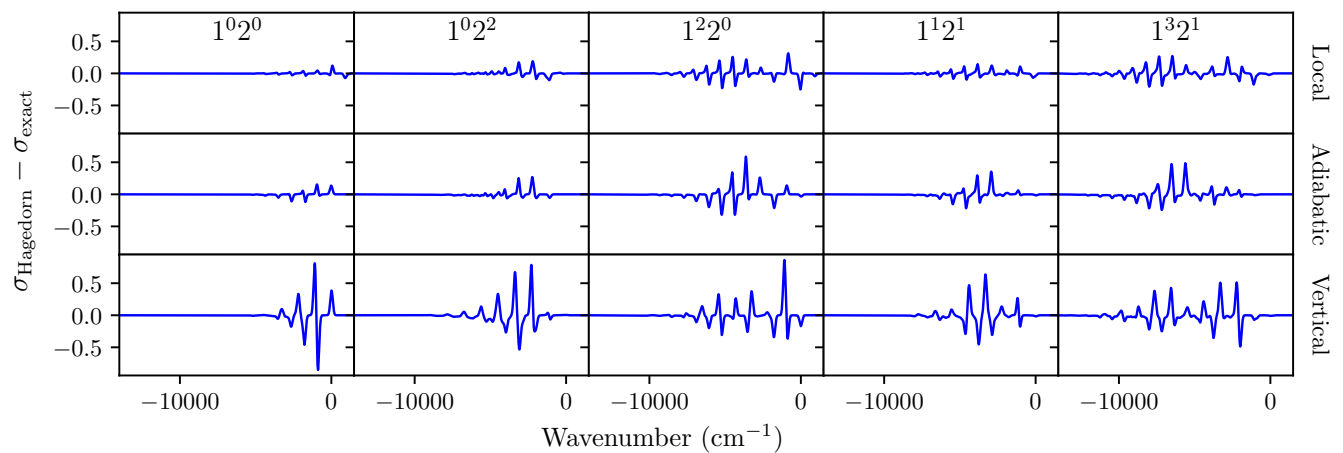


FIG. 4. Differences ($\sigma_{\text{Hagedorn}} - \sigma_{\text{exact}}$) between the SVL spectra of a two-dimensional coupled Morse potential computed with Hagedorn wavepacket dynamics and the corresponding exact spectra. See the caption of Fig. 3 for more details.

1 is excited (compare the second and third columns of Figs. 3 and 4 for $1^0 2^2$ and $1^2 2^0$ spectra). This is consistent with the fact that mode 1 is more “anharmonic” than mode 2 based on our parametrization ($\chi_1 > \chi_2$).

In general, the vertical harmonic model performs worse than the adiabatic harmonic model and the local harmonic approximation, particularly in terms of peak positions. The spectra from the adiabatic model capture the high frequency peaks in the more harmonic regions more accurately, whereas the local harmonic dynamics reproduces better the peaks in the more anharmonic low-frequency tail region. For example, in the $1^3 2^1$ spectra, the adiabatic model agrees well with the quantum result for the peaks in the region $> -5000 \text{ cm}^{-1}$ but the LHA is better at lower wavenumbers.

C. Twenty-dimensional coupled Morse potential

Since the propagation (9) of Hagedorn wavepackets with a local harmonic potential requires only propagating the five parameters of the Gaussian, the same method can be used in high-dimensional systems where exact quantum calculations are no longer practical. We therefore present a twenty-dimensional coupled Morse system as an example where split-operator benchmarks are not feasible due to the exponential scaling of the required numerical grid with D . We chose to excite at most two vibrational modes (modes 1 and 2) in the excited electronic state and computed SVL spectra from levels $1^0 2^0$, $1^0 2^3$, $1^1 2^0$, $1^1 2^1$, and $1^2 2^1$. The parameters of the simulation are given in the supplementary material.

The SVL spectra obtained from the local harmonic dynamics are compared to the adiabatic and vertical har-

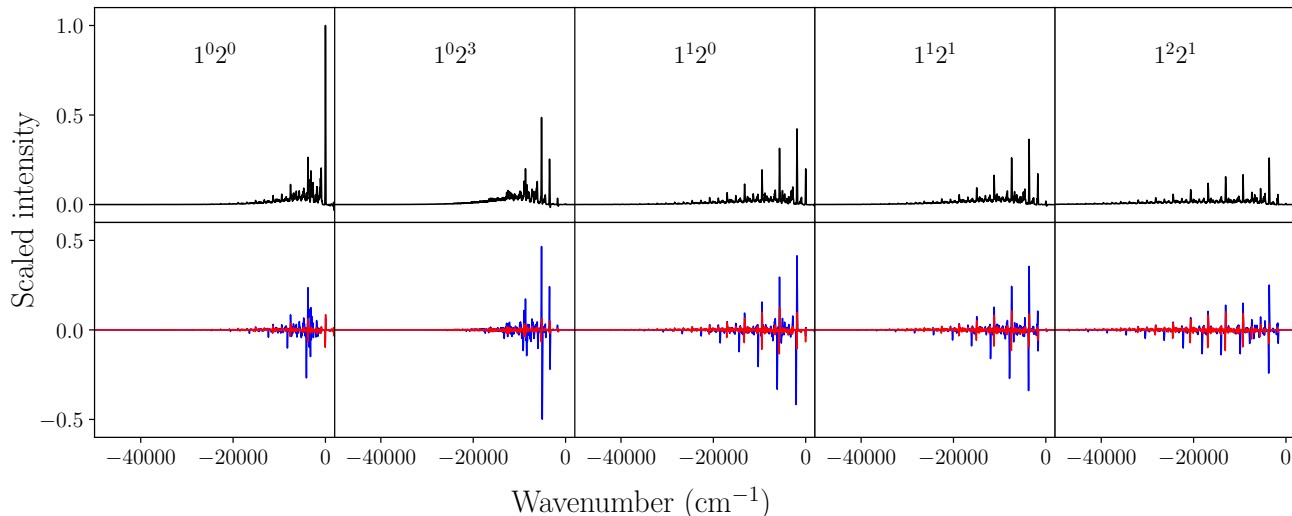


FIG. 5. SVL spectra computed with the local harmonic Hagedorn dynamics (in black) in a twenty-dimensional coupled Morse potential; below each spectrum, the differences between the local harmonic spectrum and the spectra of the adiabatic (in red) and vertical (in blue) harmonic models are shown.

monic spectra in Fig. 5. As in the lower-dimensional examples, the local harmonic results are closer to those of the adiabatic harmonic model than to the vertical one. Although the exact quantum benchmarks are not available, we can still observe significant alterations in the spectra due to the partial inclusion of anharmonicity through the local harmonic dynamics.

IV. CONCLUSIONS

We have demonstrated that the local harmonic Hagedorn wavepacket dynamics can capture anharmonic effects in SVL fluorescence spectra of moderately anharmonic and even nonseparable systems with relatively low vibrational excitations in one or multiple modes. As the initial vibrational excitation increases, the delocalization of excited vibrational wavepackets increases the effects of anharmonicity on the spectra. Although the differences between the exact and the local harmonic spectra become more pronounced for higher initial excitations, the LHA offers notable improvements over vertical and adiabatic harmonic approximations. The Hagedorn wavepacket dynamics, combined with the global or local harmonic approximation, has the advantage of obtaining SVL spectra from all initial vibrational levels using a single common Gaussian wavepacket trajectory, thus avoiding the need of repeating expensive electronic structure calculations for different initial excitations.

The local harmonic Hagedorn approach can be particularly valuable for simulating the SVL spectra of relatively small and flexible molecules, where anharmonicity is expected to play a greater role.^{17,50,51} To further increase the efficiency of the local harmonic Hagedorn approach,

techniques like Hessian interpolation³⁴ or the single Hessian approximation³⁷ could be employed, similar to their use in simulating conventional absorption and emission spectra from ground vibrational levels with the thawed Gaussian approximation. Finally, in cases where the exact spectra are completely out of reach, the local harmonic results can serve as a check of the adequacy of harmonic models.^{38,52,53}

SUPPLEMENTARY MATERIAL

The supplementary material contains the parameters of the twenty-dimensional system from Section III C.

ACKNOWLEDGMENTS

The authors acknowledge the financial support from the EPFL.

AUTHOR DECLARATIONS

Conflict of Interest

The authors have no conflicts to disclose.

DATA AVAILABILITY

The data that supports the findings of this study are available within the article and its supplementary material.

- ¹C. Parmenter and M. Schuyler, in *Transitions non radiatives dans les molécules : 20e réunion de la Société de chimie physique, Paris, 27 au 30 mai 1969* (Société de chimie physique, 1970) p. 92.
- ²W. R. Lambert, P. M. Felker, and A. H. Zewail, *J. Chem. Phys.* **81**, 2209 (1984).
- ³P. M. Felker and A. H. Zewail, *J. Chem. Phys.* **82**, 2975 (1985).
- ⁴Y. Numata, Y. Suzuki, and I. Suzuka, *J. Photochem. Photobiol. A* **237**, 49 (2012).
- ⁵M. Quack and M. Stockburger, *J. Mol. Spectrosc.* **43**, 87 (1972).
- ⁶R. Suzuki, K. Chiba, S. Tanaka, and K. Okuyama, *J. Chem. Phys.* **160**, 024301 (2024).
- ⁷J. Hollas and M. Z. Bin Hussein, *Chem. Phys. Lett.* **154**, 228 (1989).
- ⁸J. J. Newby, C.-P. Liu, C. W. Müller, and T. S. Zwier, *Phys. Chem. Chem. Phys.* **11**, 8316 (2009).
- ⁹T. C. Smith, M. Gharaibeh, and D. J. Clouthier, *J. Chem. Phys.* **157**, 204306 (2022).
- ¹⁰J. Huh and R. Berger, *J. Phys.: Conf. Ser.* **380**, 012019 (2012).
- ¹¹E. Tapavicza, *J. Phys. Chem. Lett.* **10**, 6003 (2019).
- ¹²Z. T. Zhang and J. J. L. Vaníček, “Single vibronic level fluorescence spectra from Hagedorn wavepacket dynamics,” (2024), arXiv: 2403.00577 [physics.chem-ph].
- ¹³Z. T. Zhang and J. J. L. Vaníček, “Ab initio simulation of single vibronic level fluorescence spectra of anthracene using Hagedorn wavepackets,” (2024), arXiv: 2403.00702 [physics.chem-ph].
- ¹⁴G. A. Hagedorn, *Ann. Phys. (NY)* **269**, 77 (1998).
- ¹⁵E. Faou, V. Gradinaru, and C. Lubich, *SIAM J. Sci. Comp.* **31**, 3027 (2009).
- ¹⁶C. Lasser and C. Lubich, *Acta Numerica* **29**, 229 (2020).
- ¹⁷F.-T. Chau, J. M. Dyke, E. P. F. Lee, and D. K. W. Mok, *J. Chem. Phys.* **115**, 5816 (2001).
- ¹⁸J. M. Luis, D. M. Bishop, and B. Kirtman, *J. Chem. Phys.* **120**, 813 (2004).
- ¹⁹S. Bonness, B. Kirtman, M. Huix, A. J. Sanchez, and J. M. Luis, *J. Chem. Phys.* **125**, 014311 (2006).
- ²⁰A. Galestian Pour, C. N. Lincoln, V. Perlík, F. Šanda, and J. Hauer, *Phys. Chem. Chem. Phys.* **19**, 24752 (2017).
- ²¹M. Bonfanti, J. Petersen, P. Eisenbrandt, I. Burghardt, and E. Pollak, *J. Chem. Theory Comput.* **14**, 5310 (2018).
- ²²V. Barone, S. Alessandrini, M. Biczysko, J. R. Cheeseman, D. C. Clary, A. B. McCoy, R. J. DiRisio, F. Neese, M. Melosso, and C. Puzzarini, *Nat. Rev. Methods Primers* **1**, 38 (2021).
- ²³R. Conte, C. Aieta, G. Botti, M. Cazzaniga, M. Gandolfi, C. Lanzi, G. Mandelli, D. Moscato, and M. Ceotto, *Theor. Chem. Acc.* **142**, 53 (2023).
- ²⁴J. M. Luis, B. Kirtman, and O. Christiansen, *J. Chem. Phys.* **125**, 154114 (2006).
- ²⁵J. M. Bowman, T. Carrington, and H. D. Meyer, *Mol. Phys.* **106**, 2145 (2008).
- ²⁶P. Meier and G. Rauhut, *Mol. Phys.* **113**, 3859 (2015).
- ²⁷G. J. Costa, A. C. Borin, R. Custodio, and L. N. Vidal, *J. Chem. Theory Comput.* **14**, 843 (2018).
- ²⁸S. V. Krasnoshchekov and N. F. Stepanov, *J. Phys. Chem. A* **119**, 1616 (2015).
- ²⁹M. Fusè, G. Mazzeo, G. Longhi, S. Abbate, Q. Yang, and J. Bloino, *Spectrochim. Acta A* **311**, 123969 (2024).
- ³⁰E. J. Heller, *Acc. Chem. Res.* **14**, 368 (1981).
- ³¹D. J. Tannor, *Introduction to Quantum Mechanics: A Time-Dependent Perspective* (University Science Books, Sausalito, 2007).
- ³²E. J. Heller, *J. Chem. Phys.* **62**, 1544 (1975).
- ³³F. Grossmann, *J. Chem. Phys.* **125**, 014111 (2006).
- ³⁴M. Wehrle, M. Šulc, and J. Vaníček, *J. Chem. Phys.* **140**, 244114 (2014).
- ³⁵J. Vaníček and T. Begušić, in *Molecular Spectroscopy and Quantum Dynamics*, edited by R. Marquardt and M. Quack (Elsevier, 2021) pp. 199–229.
- ³⁶M. Wehrle, S. Oberli, and J. Vaníček, *J. Phys. Chem. A* **119**, 5685 (2015).
- ³⁷T. Begušić, M. Cordova, and J. Vaníček, *J. Chem. Phys.* **150**, 154117 (2019).
- ³⁸E. Klētnieks, Y. C. Alonso, and J. J. L. Vaníček, *J. Phys. Chem. A* **127**, 8117 (2023).
- ³⁹C. Lubich, *From Quantum to Classical Molecular Dynamics: Reduced Models and Numerical Analysis* (European Mathematical Society, Zürich, 2008).
- ⁴⁰J. J. L. Vaníček, *J. Chem. Phys.* **159**, 014114 (2023).
- ⁴¹G. Hagedorn and A. Joye, *Ann. Henri Poincaré* **1**, 837 (2000).
- ⁴²R. Bourquin, V. Gradinaru, and G. A. Hagedorn, *J. Math. Chem.* **50**, 602 (2012).
- ⁴³E. Kieri, S. Holmgren, and H. O. Karlsson, *J. Chem. Phys.* **137**, 044111 (2012).
- ⁴⁴Z. Zhou, *J. Comput. Phys.* **272**, 386 (2014).
- ⁴⁵V. Gradinaru and O. Rietmann, *J. Comput. Phys.* **509**, 113029 (2024).
- ⁴⁶J. J. L. Vaníček and Z. T. Zhang, “On Hagedorn wavepackets associated with different Gaussians,” (2024), arXiv:2405.07880 [quant-ph].
- ⁴⁷R. Bourquin, *Numerical Algorithms for Semiclassical Wavepackets*, Ph.D. thesis, ETH Zürich (2017).
- ⁴⁸T. Ohsawa, *J. Fourier Anal. Appl.* **25**, 1513 (2019).
- ⁴⁹R. Moghaddasi Fereidani and J. J. L. Vaníček, *J. Chem. Phys.* **159**, 094114 (2023).
- ⁵⁰D. A. Hostutler, D. J. Clouthier, and R. H. Judge, *J. Chem. Phys.* **114**, 10728 (2001).
- ⁵¹L. Muzangwa and S. A. Reid, *J. Mol. Spec.* **310**, 105 (2015).
- ⁵²M. Wenzel and R. Mitric, *J. Chem. Phys.* **158**, 034105 (2023).
- ⁵³M. Wenzel and R. Mitric, *J. Chem. Phys.* **159**, 234113 (2023).